scientific reports

Check for updates

OPEN

Focal adhesion assembly and cell migration require myoferlin in PDAC cell lines

Charlotte Gullo[1,4], Emilie Laverdeur[1,4], Manon Dancre[1], Raphaël Peiffer[1,3], Yasmine Boumahd[1], Ferman Agirman[1], Naïma Malouhjamoum[1], Laury Désiront[1], Marc Thiry[2], Gilles Rademaker[1], Akeila Bellahcène[1] & Olivier Peulen[1]✉

Pancreatic ductal adenocarcinoma (PDAC) has a dire prognosis due to late diagnosis and ineffective treatments. Myoferlin, a transmembrane protein, is overexpressed in PDAC and correlates with poor patient survival, making it a potential therapeutic target. Several reports indicated that myoferlin depletion in cancer cells reduced migration or metastatic dissemination, but they failed to provide a consistent mechanism. Understanding the biology behind the dissemination of PDAC is of outmost importance, as this disease is often diagnosed at an advanced stage. This study aims to further elucidate myoferlin's role in cell migration. Myoferlin expression in PDAC patients correlated with gene sets related to the actin cytoskeleton, and myoferlin knockdown in PDAC cell lines similarly affected these gene sets. Electron microscopy revealed that myoferlin depletion altered cytoskeleton ultrastructure. Immunofluorescence confirmed that myoferlin knockdown disorganized microfilaments, despite not altering β-actin abundance. Functionally, myoferlin depletion significantly reduced PDAC cell migration. While core machinery for actin polymerization/depolymerization and EMT markers remained unaffected, myoferlin knockdown increased the abundance of focal adhesion components. However, immunofluorescence showed a decrease in the number of functional focal adhesions, with paxillin accumulating in the cytosol. Cell migration relies on the dynamics of focal adhesions. The reduction in functional focal adhesions indicates that the cell has fewer points of attachment for migration. We suggest this impairment was linked to a significant decrease in clathrin heavy chain abundance and pointed to a disrupted clathrin-mediated endocytosis. This study highlights a novel role for myoferlin in focal adhesion recycling in PDAC and provides a consistent mechanism explaining how myoferlin contributes to PDAC cell migration, a significant event in metastatic dissemination, and reinforce its potential as a therapeutic target.

Keywords Myoferlin, Focal adhesion, Pancreatic cancer

The mortality rate of pancreatic ductal adenocarcinoma (PDAC) is currently almost equal to its incidence[1] and its 5-year survival rate is among the lowest[2]. This dismal prognosis is mainly due to a diagnosis at an advanced stage, when dissemination has already occurred, and to the relative ineffectiveness of current treatments. Therefore, a deep understanding of pancreatic tumor biology could reveal the clues for the development of innovative and effective treatments.

Among the emerging mechanisms relevant to explain PDAC severity lies myoferlin considered as a potential oncoprotein. Myoferlin is a transmembrane protein encoded by *MYOF* gene and first described in myoblasts where it has an important function in membrane biology through its C2-mediated Ca^{2+} interaction. Myoferlin is overexpressed in PDAC[3] where it is essential to support tumor growth[4]. Moreover, myoferlin expression level correlates with low survival of PDAC patients[5,6]. Functional studies demonstrate that myoferlin was essential for exocytosis[4], while others reported its role in endocytosis[7]. The increasing therapeutic potential of myoferlin prompted researchers to develop pharmacological compounds targeting this protein. The experimental C2 domain-binding compounds showed promising anti-metastatic effects in breast cancer, colon cancer and PDAC[8–11]. This agrees with our previous report showing that myoferlin was required for PDAC dissemination to the liver[12]. Recently, we demonstrated that one of the experimental compounds targeting myoferlin, WJ460,

[1]Metastasis Research Laboratory, GIGA Institute, University of Liège, 4000 Liège, Belgium. [2]Cellular and Tissular Biology Laboratory, GIGA Institute, Université de Liège, 4000 Liège, Belgium. [3]Present address: Personalized Oncology Division, The Walter and Eliza Hall Institute of Medical Research, Parkville, Australia. [4]Charlotte Gullo and Emilie Laverdeur are shared first authorship. ✉email: olivier.peulen@uliege.be

recapitulates myoferlin gene depletion in PDAC cell lines and sensitized PDAC cell lines to ferroptosis[13]. Interestingly, ferroptosis induction completely abrogates metastasis in an orthotopic PDAC mice model[14]. This discovery encouraged us to decipher the role of myoferlin in cell migration and its therapeutic potential in metastatic PDAC.

Material and methods

Cell lines and cell culture

Human pancreatic cancer cells Panc-1, BxPC-3, MiaPaCa-2 were purchased from ATCC (Manassas, VA). Panc-1 cells were cultured in Dulbecco's modified Eagle's medium (DMEM, Lonza, Basel, Switzerland) supplemented with 10% fetal bovine serum (FBS), 1X non-essential amino acids and 2 mM L-glutamine. MiaPaCa-2 were maintained in DMEM supplemented with 10% FBS, 1 mM sodium pyruvate, and 4 mM L-glutamine. BxPC-3, cells were cultured in RPMI 1640 medium enriched with 2.5 g/L glucose, 1 mM sodium pyruvate and 10% FBS. Mycoplasma contamination was checked monthly by analyzing the activity of acetate kinase and carbamate kinase in cell culture media. In brief, enzyme substrates (3 mM acetyl phosphate, 3 mM carbamoyl phosphate), 5 µM ADP, 2 mM AMP, 3 mM magnesium acetate, 3 mM inorganic pyrophosphate, and 0.25% Triton X-100 were added to 50 µl culture media. The resulting ATP production was assessed by firefly luciferase activity. Cells were used between passage 1 and 10.

Myoferlin knockdown

Transient myoferlin knockdown was achieved with 20 nM (Panc-1 and MiaPaCa-2) or 40 nM (BxPC-3) myoferlin-specific siRNA (Eurogentec, Seraing, Belgium—siRNA MYOF#1 CCCUGUCUGGAAUGAGAUU T; siRNA MYOF#2 GAAAGAGCUGUGCAUUAUAAA; siRNA MYOF#3 GAUUGAGGGCCGACAGUUA), or a control luciferase-specific siRNA (irrelevant siRNA CUUACGCUGAGUACUUCGAT) transfected using calcium phosphate, except for BxPC-3 transfected using lipofectamine.

Whole-genome transcriptomic profiling

mRNA library was generated from 5×10^5 Panc-1 cells seeded as 3 biological replicates. Myoferlin knockdown was performed using siRNA MYOF#1. Total RNA was extracted using the NucleoSpin RNA plus kit (740984, Macherey–Nagel), according to manufacturer's recommendations. RNA quality was assessed by determining RNA integrity numbers for each sample using the Agilent RNA 6000 Nano kit (5067-1511, Agilent). Next, a mRNA library was generated using the Illumina stranded mRNA Prep Ligation kit (20040532, Illumina) according to manufacturer's instructions and sequencing was performed on an Illumina Novaseq6000 using a S4 flowcell with a depth of 2×20 M reads of 150 bp per sample.

Bioinformatics and GSEA analysis

Transcriptomic and clinical data from TCGA-PAAD (DbGAaP: phs000178, BroadGDAC: PAAD) patients[15] was retrieved from cBioportal (https://www.cbioportal.org). Patients with available mRNA expression data (n = 177) were segregated into 2 groups based on median z-score normalized *MYOF* expression. The choice of a median stratification was based on its direct clinical applicability. Differentially expressed genes, including log2FC and q-value, were obtained by comparing high *MYOF* patients with low *MYOF* patients in cBioportal. Wu's signature was applied to TCGA-PAAD patients through the PDAC gene expression visualization tool (https://pdacr.bmi.emory.edu). Patients were sorted in the heatmap according to the signature. Genes were clustered by the Euclidian method.

Further processing of transcriptomic data was performed in R (v4.4.3) and gene set enrichment analysis (GSEA) of differentially expressed genes ($p < 0.05$) was carried out using the R packages clusterprofiler (v4.14.6) and enrichplot (v1.26.6).

Ultrastructural analysis

Cells were fixed for 90 min at room temperature with glutaraldehyde (2.5%) in a Sörensen phosphate buffer (0.1 M, pH 7.4) and postfixed for 30 min with 2% osmium tetroxide. Samples were dehydrated in graded ethanol and embedded in Epon. Thanks to a Reichert Ultracut S ultramicrotome, ultrathin sections were obtained and contrasted with uranyl acetate and lead citrate. Acquisitions were performed using a Jeol (Tokyo, Japan) JEM-1400 transmission electron microscope at 80 kV. Random fields were photographed using an 11-megapixel camera system (Quemesa, Olympus). Morphometric measurements were performed and analyzed with iTEM 5.2 (Olympus, Tokyo, Japan).

RT-qPCR

Total RNA was isolated as described above. cDNA was synthesized using 4 µg RNA mixed with 1 µM random hexamer primers (SO142, Thermo) and incubated at 65°C for 5 min. Mixture was then added with M-MLV RT buffer (M5312, Promega), RNase inhibitor (EO0381, Thermo) at 2 U/µL, dNTP mix (R0191, Thermo) at 0.5 mM each and M-MLV reverse transcriptase (M1701, Promega) at 10 U/µL. Reverse transcription was performed by incubating the mix for 5 min at 25°C, 60 min at 42°C and 5 min at 70°C. qPCR was performed in 96-well plates (AB1400, Thermo). For every reaction, 100 ng cDNA was mixed with 1 µM forward and reverse primers (Supplemental Table 1) in Takyon Low ROX SYBR master mix (UF-LSMT-B0701, Eurogentec). Plates were read on a QuantStudio Real-Time PCR system (A28567, Applied Biosystems). Amplification conditions were initiated with 10 min denaturation at 95°C, followed by 40 cycles of 15s denaturation at 95°C and 1 min annealing/elongation at 60°C. Results were analyzed using the ΔΔCT method, 18S ribosomal RNA was used for normalization.

Western blot

Cells were lysed in 1% sodium dodecyl sulfate added with protease (3 µM aprotinin, 80 µM leupeptin, 60 µM pepstatin A and 40 µM PMSF) and phosphatase (5 mM NaF, 1 mM Na3VO4) inhibitors. Protein concentration was determined using the Pierce BCA protein assay kit (23227, Thermo). Western blots were performed as described previously[16]. Primary antibody list is available (Supplemental Table 2).

Immunofluorescence and microfilament staining

Cells (4×10^4) were seeded on glass coverslips. After overnight attachment, cells were fixed using 4% paraformaldehyde for 10 min at room temperature. Cells were then permeabilized (PBS 1% Triton X-100) for 5 min and blocked (PBS-BSA 1%) for 30 min. Primary antibodies (Supplemental Table 2) were diluted 1/100 in PBS-BSA 1%, and coverslips were incubated overnight at 4°C. After washing, fluorescent secondary antibodies (Supplemental Table 2) were diluted 1/1000 in PBS-BSA 1% with 1 µg/mL Hoechst 33258 (H1398, Thermo), coverslips were incubated for 45 min at room temperature. For cytoskeleton imaging, cells were stained with Phalloidin following manufacturer's instructions (R415, Invitrogen). Finally, coverslips were mounted onto glass slides using fluorescence mounting medium (S3023, Agilent-Dako). Coverslips were imaged on a Nikon A1R or Leica Stellaris 8 confocal microscope using a 40× or 63× oil-immersion objective. Image analysis was performed on raw images using Fiji (v2.16.0) 1.54 p and LUSCA (v1.1.0) plugin.

Migration assays

Scratch assay was performed using Incucyte S3 (Sartorius, Ann Arbor, Mi). Cells were seeded (Panc-1 40,000 cells/well, MiaPaCa-2 90,000 cells/well, BxPC-3 60,000 cells/well) the day before experiment to achieve confluence the day of experiment. Scratches were then applied to cells using the Sartorius wound maker tool. To avoid proliferation bias, migration was only evaluated during 24 h, corresponding to the half of the cell doubling time. Results were expressed as the relative wound density (%), corresponding to the percentage of cell confluence in the wound in comparison with cell confluence outside of the wound. For Boyden's chamber migration, cells were resuspended in DMEM with 1% bovine serum albumin (BSA) and seeded on trans-well inserts (8 µm pore size—Panc-1 100,000 cells/well, MiaPaCa-2 30,000 cells/well, BxPC-3 150,000 cells/well). Chemoattractant (10% FBS) was placed in the bottom compartment. Cells were allowed to migrate during 24h before fixation and staining with Diff-Quick reagents (CellaVision, Lund, Sweden). Migrating cells were counted at the bottom side of the trans-well using CellProfiler (v4.2.5).

Statistical analysis

Statistical analyses were carried out in GraphPad Prism (v10). Quantitative variables were compared using Student t-test or one-way ANOVA (including Dunnet's multiple comparisons) according to the number of experimental groups. Kinetic of cell migrations were compared after a third order polynomial curve fitting using least square regression. Fitting parameters were compared by sum of squares F test. Additionally, 2-way ANOVA were performed to evaluate main effects (time and siRNA) and interaction effect. Statistical significance for all experiments was defined as $p < 0.05$.

Results

Myoferlin expression correlates with expression of actin cytoskeleton gene sets in PDAC patients and myoferlin knockdown PDAC cells

To determine whether myoferlin is involved in metastasis, we applied a PDAC metastasis-related gene expression signature[17] on 177 PDAC patients available in the TCGA PanCancer Atlas study. Interestingly, the 246 genes signature associated the PDAC patients with the highest *MYOF* expression with the high metastatic signature (Supplemental Fig. S1). To avoid an overfitting bias, a derived signature reduced to 7 genes was constructed by a LASSO-Cox regression model[17] and applied with similar results (Fig. 1A). While not included in the metastasis signatures, the myoferlin gene expression was significantly correlated with the metastasis signature (Fig. 1B and Supplemental Fig. S1). We then segregated the population of PDAC patients based on myoferlin expression. The segregation strategy was based on the use of the myoferlin median Z-score relative to all samples in the cohort. The groups termed "high *MYOF*" (RSEM batch normalized: 7878.37) and "low *MYOF*" (RSEM batch normalized: 3426.56) comprised 89 and 88 patients, respectively. We then evaluated the number of patients with lymph nodes colonization (N1 and N1B) according to the TNM stages in each group (Fig. 1C). Significantly more patients with lymph node invasion were present in "high *MYOF*" group. The gene expression data from the tumors of these patients, obtained through bulk RNA sequencing (RNA-seq), were subjected to gene set enrichment analysis (GSEA). This analysis revealed 128 ontology terms related to cellular components that were significantly modulated between the two groups. According to the proportion of genes within a pathway that are also part of the differentially expressed gene set, the group of genes involved in the actin cytoskeleton (GO:0015629) was ranked within the top 20 of the most activated (rank 12 with NES > 0—Fig. 1D). The GSEA analysis assigned it a normalized enrichment score (NES) of 1.83 (adjusted p-value = 0.0002). Additionally, several child terms were also significantly modulated but below the top 20: actin filament (GO:0005884, NES = 1.92, adjusted p-value = 0.008), actin filament bundle (GO:0032432, NES = 2.07, adjusted p-value = 0.002), contractile actin filament bundle (GO:0097517, NES = 1.88, adjusted p-value = 0.018), actomyosin (GO:0042641, NES = 1.77, adjusted p-value = 0.015), stress fiber (GO:001725, NES = 1.88, adjusted p-value = 0.015) (Supplemental Fig. S1. We then determined whether the expression of genes coding for different actins was modulated in the two patient groups. It appeared that the genes *ACTA2* (α-smooth muscle actin 2, $p = 0.0009$), and *ACTB* (β-actin, $p < 0.0001$) were significantly more expressed in the "high *MYOF*" group. In contrast, *ACTG1* (γ-actin 1, $p = 0.0077$) and *ACTC1* (α-cardiac muscle actin, $p = 0.0458$) were significantly less expressed there (Fig. 1E and Supplemental

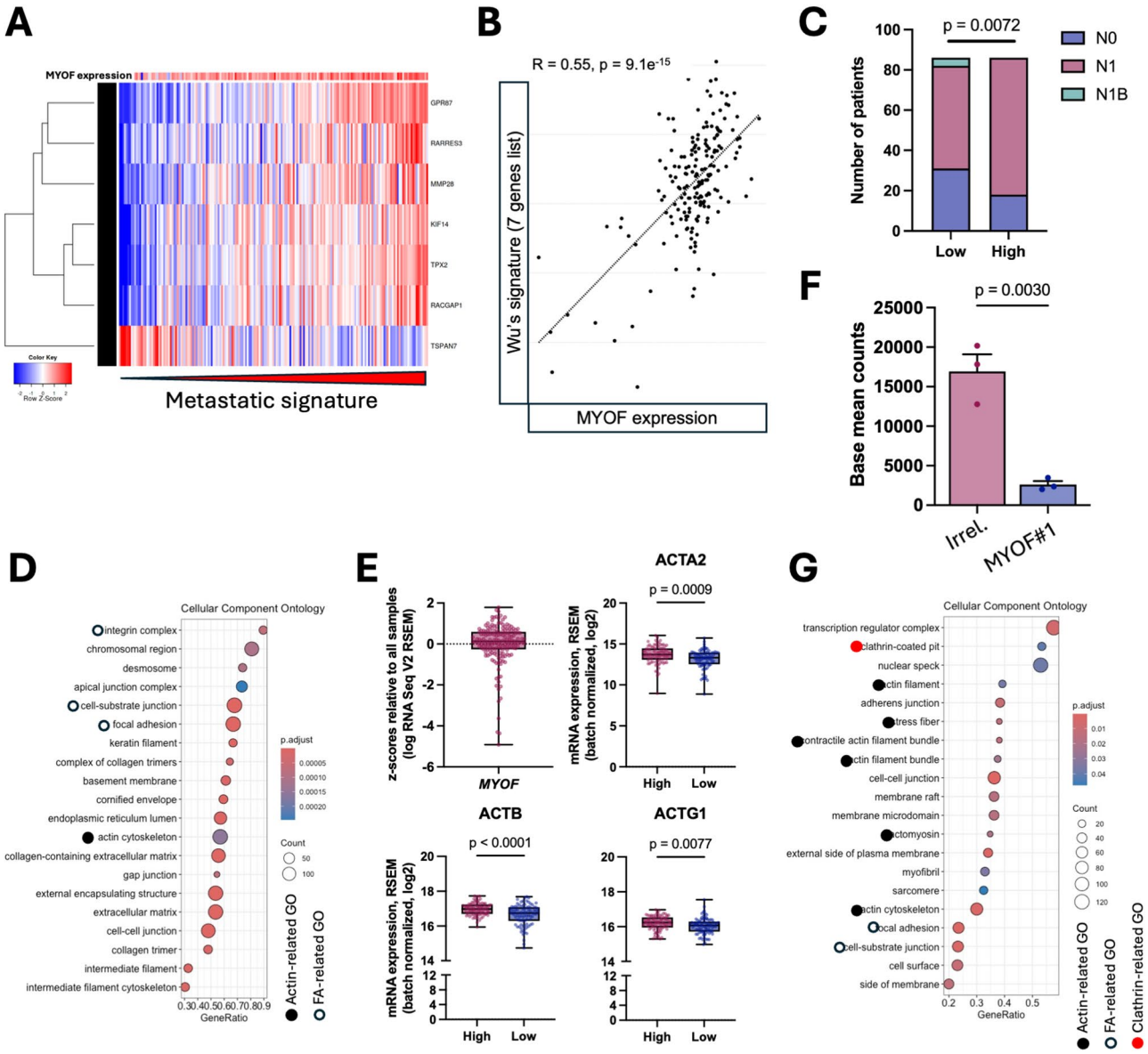

Fig. 1. Myoferlin expression correlates with expression of actin cytoskeleton gene sets in PDAC patients and myoferlin knockdown PDAC cells. (**A**) Heatmap and unsupervised clustering of a 7 gene metastatic signature in PDAC TCGA patients (n = 177). Gene expression values are z-score normalized. (**B**) Correlation between *MYOF* gene expression and average expression of 7 genes included in a metastatic signature in PDAC TCGA patients (n = 177). (**C**) Repartition of N0 (no lymph node infiltration), N1 (one lymph node infiltrated) and N1B (several lymph nodes infiltrated) PDAC TCGA patients according to high and low *MYOF* groups. Chi-square test. (**D**) GSEA results of differentially expressed genes ($p < 0.05$) in high and low *MYOF* groups. Genesets extracted gene ontology (GO—cellular component ontology). (**E**) RNAseq-based *MYOF*, *ACTA2*, *ACTB*, *ACTG1* expression in PDAC TCGA cohort patients (n = 177) according to *MYOF* expression. Boxplot, unpaired Student's t test. (**F**) RNAseq-based *MYOF* expression in Panc-1 cells transfected with irrelevant (Irrel.) or myoferlin specific (MYOF) siRNA. **G** GSEA results of differentially expressed genes in Panc-1 cells transfected with myoferlin specific (MYOF) siRNA. Genesets extracted gene ontology (GO—cellular component ontology).

Fig. S1). The genes coding for *ACTA1* (α-smooth muscle actin 1) and *ACTG2* (γ-smooth muscle actin 2) were not significantly modulated (Supplemental Fig. S1).

Encouraged by the previous results, we utilized bulk RNA-seq data generated from PDAC cells, specifically the Panc-1 cell line, in which the expression of myoferlin was reduced (Fig. 1F) following the transfection with small interfering RNAs (siRNA). These data underwent GSEA analysis. Several gene sets involved in actin cytoskeleton were among the top enriched ontology terms when myoferlin was depleted (Fig. 1G and Supplemental Fig. S1): actin cytoskeleton (GO:0015629, NES = 1.77, adjusted *p*-value = 0.003), actin filament bundle (GO:0032432, NES = 2.00, adjusted *p*-value = 0.018), contractile actin filament bundle (GO:0097517,

NES = 2.12, adjusted p-value = 0.009), actomyosin (GO:0042641, NES = 2.00, adjusted p-value = 0.019), stress fiber (GO:001725, NES = 2.12, adjusted p-value = 0.009). However, expression of specific actin genes was either barely detectable (*ACTA1*, *ACTA2*, *ACTC1*, *ACTG2*), or not significantly impacted (*ACTB*, *ACTG1*) by myoferlin knockdown (Supplemental Fig. S1).

It therefore appears clear that, both in patients and in a pancreatic cancer cell line, the level of expression of myoferlin is associated to the expression of genes related to the actin cytoskeleton, while actin genes were not necessarily modulated. We propose that the observed enrichment of the actin cytoskeleton gene set was most likely driven by an expression correlation between *MYOF* and genes encoding key actin cytoskeleton associated proteins.

Myoferlin knockdown tampers cytoskeleton ultrastructure in PDAC cells

Three PDAC cell lines (Panc-1, MiaPaCa-2 and BxPC-3) were knocked down for myoferlin and submitted to transmission electron microscopy. The cytoplasm of cells transfected with an irrelevant siRNA contained sections within elements of the endomembrane system, including rough endoplasmic reticulum, as well as abundant elongated mitochondria. The cytoplasm also contained occasional intertwined fragments of a cytoskeleton of undefined nature (Fig. 2A and Supplemental Fig. S2). When myoferlin was depleted, the cytoplasm contained large areas that were very dense with cytoskeletal elements, while other regions seemed to lack them. Precise measurement of the diameter of these fibrillar elements was performed at 30,000× magnification. The fiber diameter was 8.2 ± 1.1 nm, pointing to microfilaments (Fig. 2B). This observation suggests a modification in the structure of these cytoskeletal elements when myoferlin is no longer present.

Myoferlin knockdown disorganizes microfilaments but do not alter β-actin abundance

To shed light on the nature of the cytoskeleton affected by myoferlin knockdown, we analyzed the abundance of β-actin, lamin B1, vimentin and α-tubulin belonging to different cytoskeletal categories. The three siRNAs reduced myoferlin abundance up to 90%. It appeared that neither the abundance of β-actin, lamin B1, vimentin and α-tubulin (Fig. 2C and Supplemental Fig. S2) nor the corresponding gene expression (Supplemental Fig. S2) were altered by myoferlin depletion. We therefore sought to highlight the cellular distribution of actin cytoskeleton using FITC-conjugated phalloidin, a dye specific to fibrillar actin structures (Fig. 2D and Supplemental Fig. S2). Confocal microscopy images revealed numerous actin fibers in cells transfected with an irrelevant siRNA, and these fibrous structures were shorter 48h after myoferlin knockdown (Fig. 2E). However, labeling remained present and was distributed throughout the cytoplasm or at the plasma membrane (arrowheads). Collectively, our results suggest that the abundance of β-actin monomers was not influenced by myoferlin depletion, while microfilaments architecture was strongly affected. The long fibers observed in non-depleted cells can be related to actin stress fibers. They are contractile bundles found in non-muscle cells and play an important role in cell contractility. They provide the force necessary for cell adhesion and migration. Interestingly, the gene sets involved in these ontology terms (stress fiber—GO:001725, contractile actin filament bundle—GO:0097517, actin filament bundle—GO:0032432, and actomyosin—GO:0042641) were significantly activated after myoferlin depletion (Fig. 1C,F).

Myoferlin knockdown reduces PDAC cell migration

Since these structures play a role in cell migration and our work focusses on a metastatic disease, we considered it was appropriate to analyze cell migration after myoferlin depletion. First, we performed a wound healing assay during 24h. We observed a significant decrease in the migration speed of cancer cells when myoferlin was depleted. Indeed, the relative wound density was about 60% in Panc-1 transfected with irrelevant siRNA while approximatively 30% and 40% when cells where transfected with myoferlin siRNA#1 and siRNA#2 respectively (Fig. 3A). Significant reductions were also observed in myoferlin-depleted BxPC-3 cell line while the migration kinetic profiles were different from the ones observed in Panc-1 cells (Supplemental Fig. S3). Indeed, BxPC-3 cells appeared to undergo a retraction step before migration. MiaPaCa-2 cell line migrated more slowly than the two other cell lines explaining probably why myoferlin-knockdown did not impact their migration. These specific migration patterns were in accordance with what we previously reported[12]. We then evaluated chemotaxis migration of Panc-1 in Boyden chambers where myoferlin silencing led to a 25% and 45% reduction with myoferlin siRNA#1 and siRNA#2 respectively (Fig. 3B). Similar reductions were observed in BxPC-3 and MiaPaCa-2 cell lines when myoferlin was depleted with siRNA#1 (Supplemental Fig. S3).

At this stage of our work, we have shown that myoferlin depletion causes a profound modification of the actin cytoskeleton structure, which correlates functionally into a reduction in the migration capabilities of PDAC cells.

Myoferlin knockdown does not modify abundance of microfilaments dynamics machinery core components

To elucidate the mechanisms by which myoferlin depletion alters the actin cytoskeleton we have evaluated the abundance of proteins regulating actin dynamics, namely polymerization and depolymerization. First, cofilin (or ADF) which controls F-actin depolymerization according to its phosphorylation state. Second, SSH1 (Slingshot homolog 1) which is a cofilin-activating phosphatase. Third, LIMK1 (LIM domain kinase 1) protein, active in phosphorylated form, is a cofilin-inhibiting kinase. It appeared that neither cofilin and phospho-cofilin (S3) abundance, nor the ratio of the phosphorylated form to the total form of the protein were altered upon myoferlin depletion by MYOF#1, #2 or #3 siRNAs (Fig. 3C and Supplemental Fig. S3). Following the same reasoning, the abundances of SSH1 (Fig. 3D and Supplemental Fig. S3) and LIMK1 (Fig. 3E and Supplemental Fig. S3) were not significantly modulated by myoferlin depletion. We were unable to detect the phosphorylated form of LIMK1 (T508). These results highlight that despite a clear disorganization of actin microfibers; the core machinery of actin polymerization/depolymerization is unaffected upon myoferlin depletion.

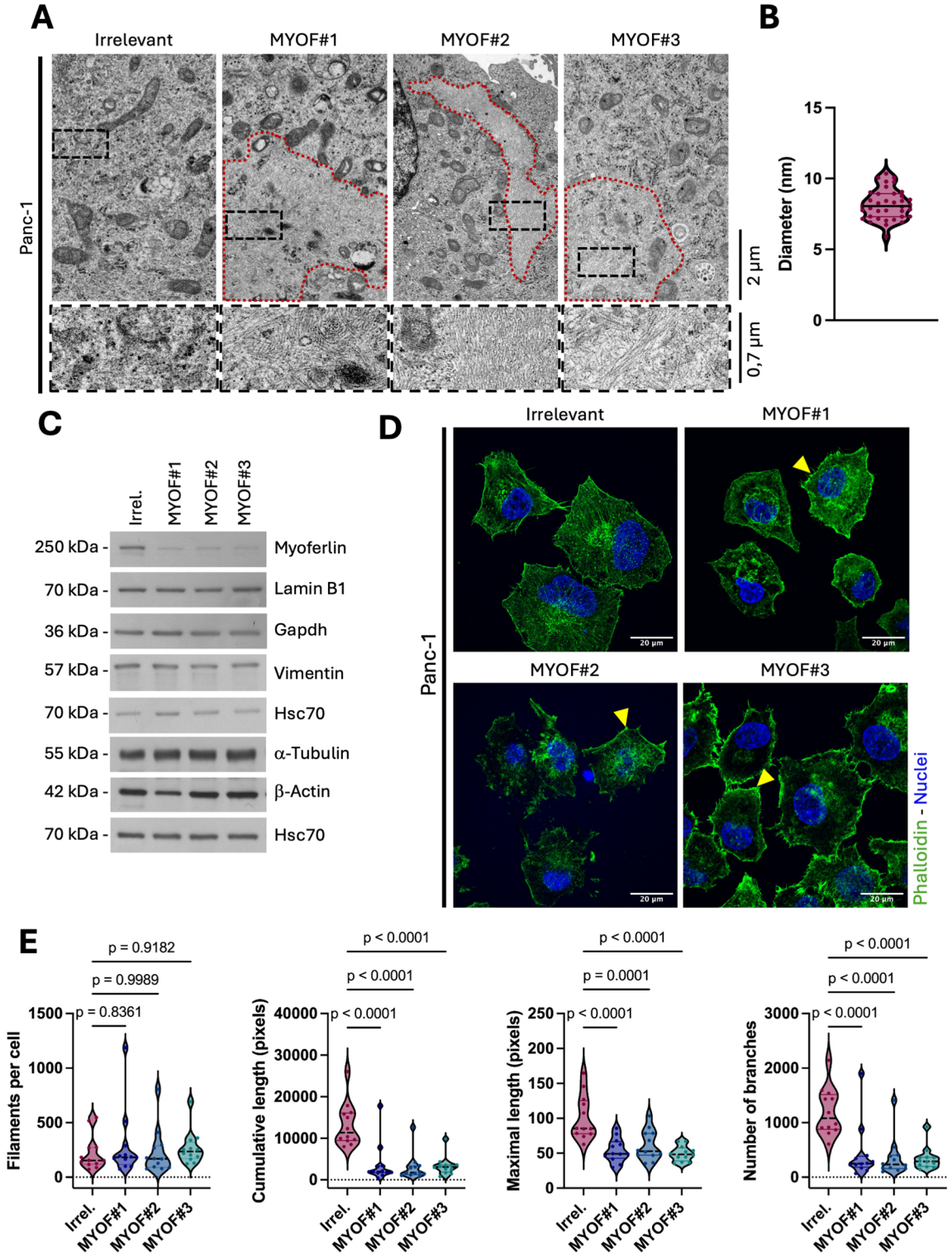

Cell migration is largely influenced by the epithelial-mesenchymal transition (EMT). This transition is estimated by evaluating the relative abundance of markers, including E-cadherin, specific to epithelial cells, and vimentin, specific to mesenchymal cells. We wondered whether, in addition to the alteration of actin microfilaments, the reduction in Panc-1 migratory capacity due to myoferlin depletion could be the result of a mesenchymal-epithelial transition, the reverse process of EMT. Our results indicated that Panc-1 cells were characterized by a mesenchymal phenotype, as evidenced by the expression of vimentin (Fig. 2C) and the absence of E-cadherin (result not shown), in combination with a high migratory capacity (Fig. 3A). This characteristic is consistent with the results we previously published[5]. Myoferlin depletion did not alter the abundance of EMT markers, indicating that a mesenchymal-epithelial transition did not took place, recapitulating our previous results[12]. This finding suggests that myoferlin's role in promoting PDAC cells migration is different from what was observed in breast cancer cells and independent of its function in the regulation of cell plasticity[18]. However,

◂**Fig. 2**. Myoferlin knockdown tampers cytoskeleton ultrastructure, disorganizes microfilaments. (**A**) Ultrastructure of Panc-1 cells transfected with irrelevant or myoferlin specific (MYOF#1, #2, #3) siRNA. Red dotted lines delimitate areas with very dense cytoskeletal elements. Scale bar = 2 µm. Black dashed lines delimitate areas represented at higher magnification. Scale bar = 0.7 µm. (**B**) Size analysis of cytoskeletal element diameter at 30,000× magnification. Fiber diameters (n = 37) were measured in MYOF#2 samples from 6 different cells. (**C**) Western blot analysis of Panc-1 total-cell lysates. One representative western blot of three independent experiments is shown HSC70 was used as loading control. (**D**) Actin filaments visualization in Panc-1 cells transfected with irrelevant or myoferlin specific (MYOF#1, #2, #3) siRNA. Yellow arrowhead pointed to F-actin accumulation at plasma membrane. Scale bar = 20 µm. (**E**) Number of actin filaments per cell (n = 12), cumulative length of filaments per cell (n = 12), maximal filament length per cell (n = 12), and number of filament branches per cell (n = 12) in Panc-1 cells transfected with irrelevant or myoferlin specific (MYOF#1, #2, #3) siRNA. Violin plot, one-way ANOVA (Dunnett's test), *p*-value relative to control group (Irrel. siRNA).

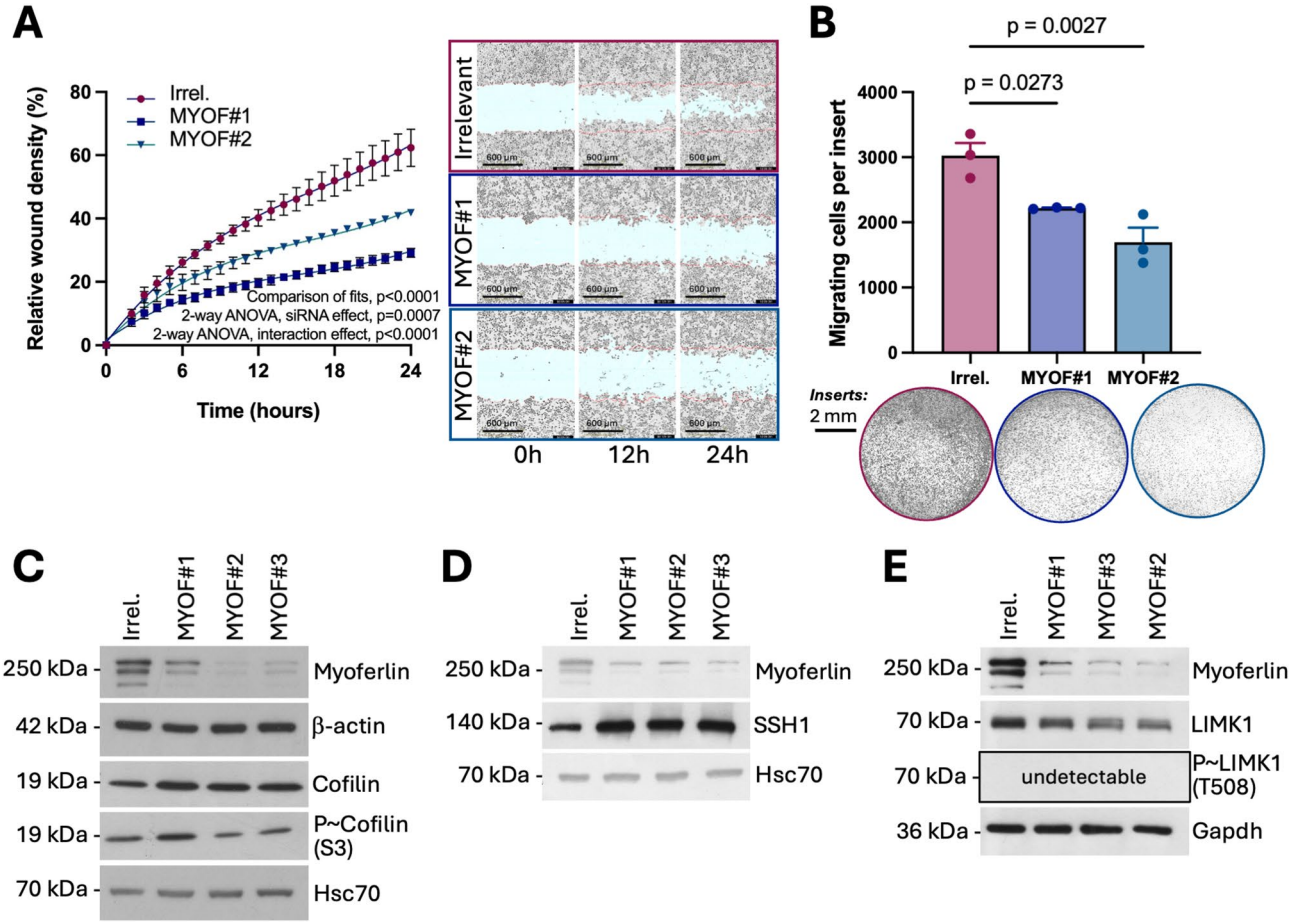

Fig. 3. Myoferlin knockdown reduces cell migration but does not modify abundance of microfilaments dynamics machinery core components. (**A**) Relative wound density (%) over time and scratch wound images (0h, 12h, 24h) of Panc-1 cells transfected with irrelevant or myoferlin specific (MYOF#1, #2) siRNA. Data were fitted according to a third order polynomial model by least square regression. Global fit parameters were compared to independent fits by the extra sum-of-square F test. Mean ± SEM, two-way ANOVA (full model including time effect, siRNA effect and interaction effect). Scale bar = 600 µm. (**B**) Quantitative and qualitative (inserts) chemotaxis migration of Panc-1 cells transfected with irrelevant or myoferlin specific (MYOF#1, #2) siRNA. Mean ± SEM, one-way ANOVA (Dunnett's test), *p*-value relative to control group (Irrel. siRNA). Scale bar = 2 mm. (**C–E**) Western blot analysis of Panc-1 total-cell lysates. One representative western blot of three independent experiments is shown HSC70 or GAPDH were used as loading control.

assessing the occurrence of a mesenchymal-epithelial transition, a gradual process, based only on the expression of two markers, albeit well-established, provides a limited perspective. A more comprehensive evaluation incorporating additional epithelial and mesenchymal markers, such as cytokeratin's, tight junction proteins, N-cadherin, and key transcription factors, would be necessary to fully characterize potential changes in cellular identity.

Myoferlin knockdown increases abundance of focal adhesion components but decreases functional focal adhesion number

Unable to correlate the migratory capacity of the cells when myoferlin is depleted with either the abundance of the microfilament dynamics machinery or the EMT process, we decided to investigate the focal adhesion complexes, pointed out by the GSEA analysis (Fig. 1D,G) both in TCGA data and Panc-1 cells depleted for myoferlin. Indeed, the cell-substrate junction (GO:003005) and focal adhesion (GO:0005925) were significantly activated (Fig. 4A).

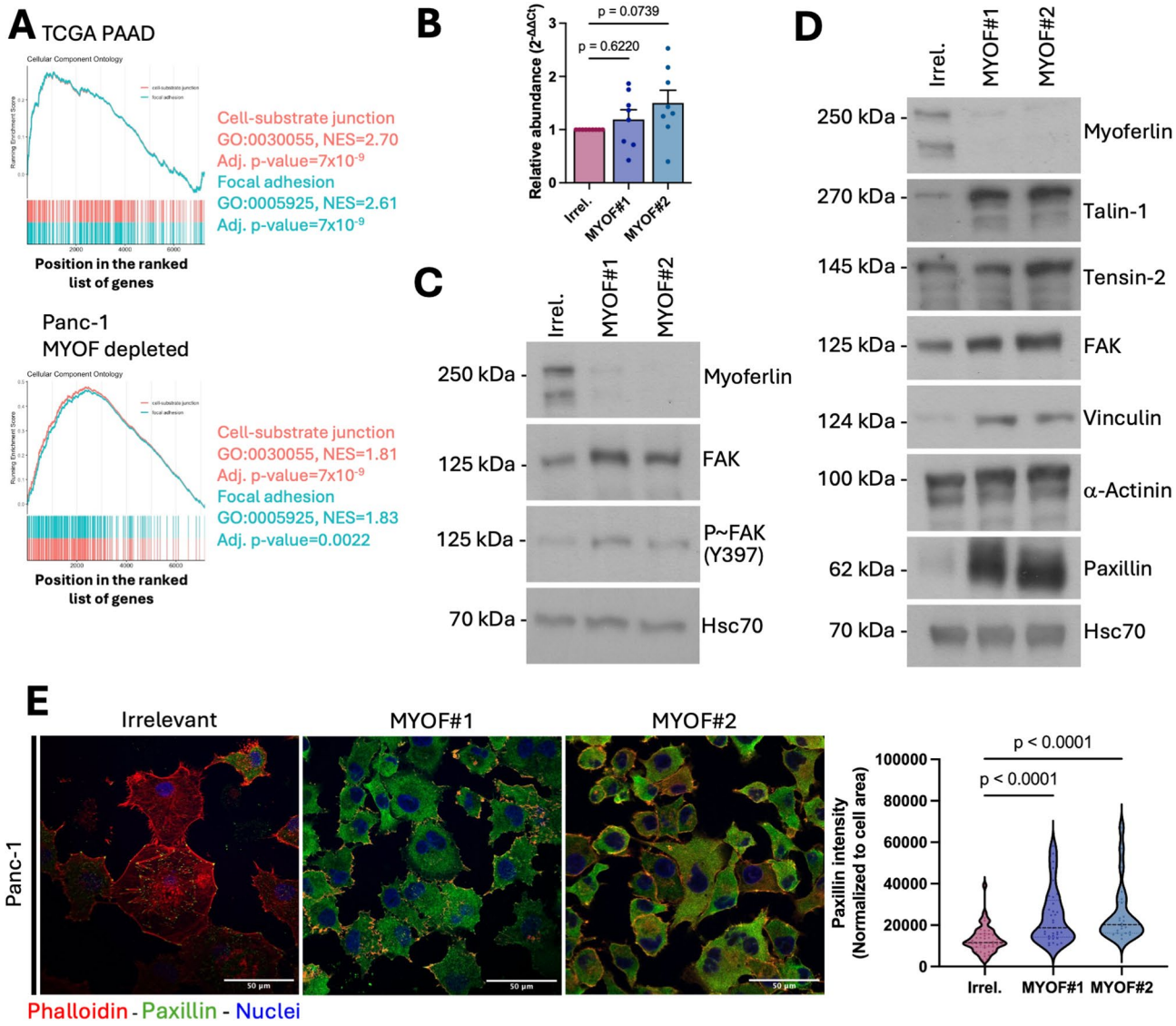

Fig. 4. Myoferlin knockdown increases abundance of focal adhesion components. (**A**) GSEA analysis of differentially expressed genes ($p < 0.05$) in PDAC TCGA cohort patients (n = 177) and Panc-1 cells transfected with irrelevant or myoferlin specific siRNA. Benjamini–Hochberg procedure. NES = normalized enrichment score. (**B**) RT-qPCR analysis of *FAK* mRNA levels in Panc-1 cells transfected with irrelevant (Irrel.) or myoferlin specific (MYOF#1, #2) siRNA (Irrel. shRNA; n = 9 each). Mean ± SEM, one-way ANOVA (Tukey's test). (**C**) and (**D**) Western blot analysis of Panc-1 total-cell lysates. One representative western blot of three independent experiments is shown HSC70 was used as loading control. (**E**) Immunofluorescent confocal microscopy of Paxillin upon myoferlin depletion in Panc-1 cells. Representative pictures are shown. Nuclei = blue, Paxillin = green, Phalloidin = red, scale bar = 50µm. Paxillin fluorescence intensity was quantified for individual cells (Irrel. n = 50; MYOF#1 n = 33; and MYOF#2; n = 22). Violin plot, one-way ANOVA (Dunnet's test), *p*-value relative to control group (Irrel. siRNA).

We thus analyzed Focal Adhesion Kinase (FAK) gene expression, protein abundance and phosphorylation in myoferlin-knockdown Panc-1 cells. Interestingly, myoferlin knockdown did not altered *FAK* gene expression (Fig. 4B), but increased systematically FAK protein abundance, and significantly its phosphorylation on tyrosine 397 residue (Fig. 4C and Supplemental Fig. S4). BxPC-3 cells underwent a similar increase when transfected with myoferlin siRNAs (Supplemental Fig. S4). Focal adhesions are large multi-protein (up to 100) structures linking actin bundles to extracellular matrix through integrin receptors. We therefore wished to determine whether the modification observed for FAK could be extended to other constituents of focal adhesions. The abundance of several proteins (talin-1, vinculin, and paxillin) was systematically increased when myoferlin was silenced (Fig. 4D), but only paxillin reached a significant and consistent increase (Supplemental Fig. S4). This increase was the result of an enhanced *PXN* gene expression (Supplemental Fig. S4). A similar protein increase was observed for paxillin in BxPC-3 and MiaPaCa-2 (Supplemental Fig. S4) cells.

Paxillin is a focal adhesion adaptor protein that acts as a scaffold, recruiting and organizing other proteins at focal adhesions. Its significant and intense increase upon myoferlin knockdown could indicate an expanded number of focal adhesions. However, immunofluorescence in myoferlin depleted cells showed that paxillin abundance was indeed increased but mainly located in the cytosol (Fig. 4E).

Focal adhesions are often considered as cell "feet", serving as attachment sites for microfilaments to plasma membrane, and essential for cell anchoring and migration. The increase in focal adhesion components suggests an increase in migration potential, which is inconsistent with our observations. We thus decided to evaluate the focal adhesion themselves and not only their components. Co-staining of vinculin and microfilaments with phalloidin showed a decrease of the average number of functional focal adhesions per cell (Fig. 5A,B and Supplemental Fig. S5), in line with the cytosolic localization of paxillin upon myoferlin knockdown.

Myoferlin knockdown impairs focal adhesion independently of paxillin phosphorylation, but concurrently with clathrin disappearance

FAK and paxillin are closely linked since FAK can phosphorylate paxillin primarily at tyrosine residues Y31 and Y118, crucial for focal adhesion dynamics and migration by promoting their disassembly[19]. Additionally, serine residue S126 phosphorylation by ERK leads to a relocalization of paxillin from focal adhesions to the cytosol[20]. Owing to the observed reduction of focal adhesion and the accumulation of paxillin in cytosol, we thought to evaluate the phosphorylation of Y31, Y118 and S126 on paxillin.

Inexplicably, we were unable to show any phosphorylation of paxillin on tyrosine Y118 and serine S126 residues in Panc-1 cell line (data not shown). However, the abundance of the phosphorylated paxillin on Y31 residue was increased by tenfold (Fig. 5C,D). In BxPC-3 and MiaPaCa-2 cell lines, our results showed that phosphorylation of Y31 residues were unchanged upon myoferlin knockdown (Supplemental Fig. S5). Unable to correlate the focal adhesion abundance to paxillin phosphorylation when myoferlin is depleted in MiaPaCa-2 and BxPC-3 cell lines, we thought to investigate a potential link with calpain-2. Calpain-2 is a calcium-dependent protease catalyzing paxillin cleavage and leading to the inhibition of cell migration and adhesion dynamics[21]. In our experimental conditions, calpain-2 remained unchanged upon myoferlin silencing (Fig. 5C and Supplemental Fig. S5).

Owing to the known function of myoferlin in plasma membrane recycling, and its described colocalization with caveolin and clathrin[22], two elements involved in focal adhesion recycling, we undertook an analysis of these proteins upon myoferlin knockdown. We observed a significant decrease of clathrin heavy chain abundance while caveolin was not modified (Fig. 5E and Supplemental Fig. S5). Immunofluorescence performed on Panc-1 cells confirmed this observation (Fig. 5F and Supplemental Fig. S5) which seemed to be unrelated to a reduction of *CLTC* gene expression (Supplemental Fig. S5). Interestingly, alteration of the clathrin-coated pit gene set was noticed by the GSEA analysis performed on bulk RNA-seq obtained from myoferlin-depleted Panc-1 (Fig. 1G, GO:0005905, NES = 1.84, adjusted p-value = 0,002). The reduced activity of the clathrin-associated endocytosis was confirmed by an accumulation of integrin β1 at the plasma membrane upon myoferlin knockdown (Supplemental Fig. S5).

Altogether, our results suggested an impairment of focal adhesion assembly and/or turnover at plasma membrane upon myoferlin knockdown in pancreatic cancer cells.

Discussion

While the role of actin microfilaments in metastatic dissemination no longer needs to be demonstrated[23], several reports showed that actin cytoskeleton participates to mitochondrial function, morphology, and subcellular localization[24,25]. Interestingly, mitochondrial subcellular localization was also reported as an essential regulator of cell dissemination[26,27]. In fact, mitochondrial trafficking to the cortical actin cytoskeleton controls tumor cell motility[28,29]. Additionally, actin-binding proteins, such as cofilin and actin-related protein 2/3, were demonstrated to participate in mitochondrial fusion/fission and mitophagy[30,31]. Owing to similar observations reported upon myoferlin depletion in PDAC cells[5,12,13], we hypothesized that myoferlin depletion could mediate its effects via an alteration of microfilaments, leading to a decrease of cell migration and potentially to a reduction of metastatic dissemination.

We demonstrated that while myoferlin knockdown resulted in a significant disorganization of microfilaments, there was neither alteration of *ACTB* gene expression, nor of β-actin abundance at protein level. This apparent discrepancy can originate from several aspects, including β-actin post-translational modifications or alteration of the structural regulation of microfilaments. β-actin post-translational modifications are potentially numerous and deserve specific investigation. Structural regulation of microfilaments involves dynamic polymerization and depolymerization controlled by various proteins. Key proteins include cofilin, that was not altered by myoferlin knockdown. Several other regulators, such as Arp2/3 proteins, formin, profilin, or capping proteins, deserve to

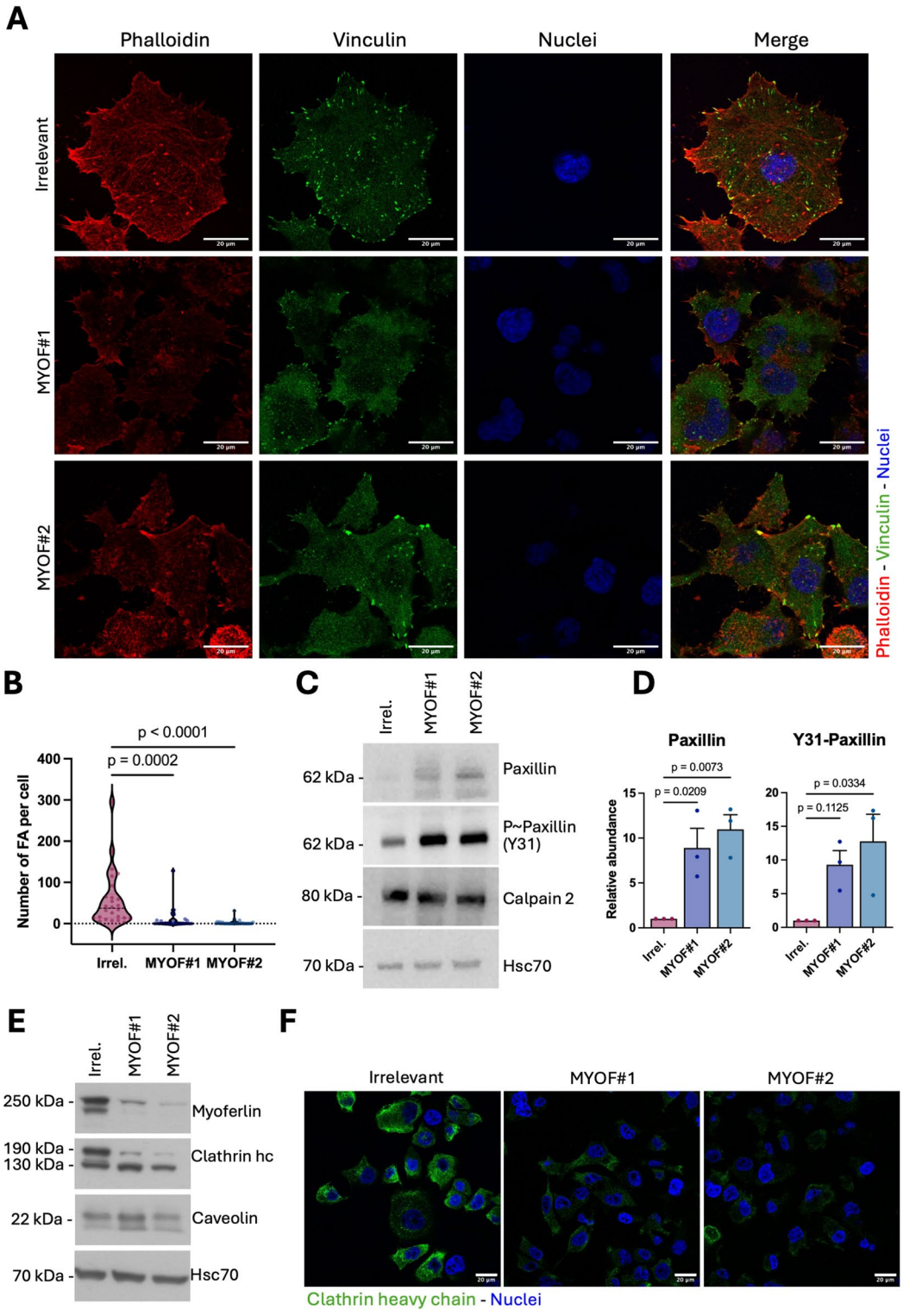

be analyzed. Microfilaments are also critically controlled by focal adhesion assembly, significantly altered by myoferlin silencing, and acting as filament-anchoring signaling centers.

Previously, myoferlin was already associated with focal adhesion. Blackstone et al. demonstrated that shRNA-mediated myoferlin knockdown in MDA-MB-231 breast cancer cells increased FAK and paxillin phosphorylation, at residues Y397 and Y118, respectively[32]. Additionally, they reported altered focal adhesion morphology with larger and elongated adhesions when myoferlin was silenced. Although not quantified, the number of focal adhesions appeared reduced. Surprisingly they described thicker and more numerous actin fibers in myoferlin depleted cells, whereas the same group previously reported fewer stress fibers and an expended cortical actin cytoskeleton under the same experimental conditions[33]. In melanoma cells, siRNA-mediated myoferlin silencing also increased FAK phosphorylation at residues Y397 and enlarged focal adhesions[34], suggesting that myoferlin may exert distinct functions across cancer types. To address these discrepancies and better understand the

◀**Fig. 5**. Myoferlin knockdown decreases focal adhesion number and clathrin abundance. (**A**) Immunofluorescent confocal microscopy of Vinculin upon myoferlin depletion in Panc-1 cells. Representative pictures are shown. Nuclei = blue, Vinculin = green, Phalloidin = red, scale bar = 20 µm. (**B**) Vinculin and phalloidin colocalisation was quantified for individual cells (Irrel. n = 30; MYOF#1 n = 23; and MYOF#2; n = 30). Violin plot, one-way ANOVA (Dunnet's test), *p*-value relative to control group (Irrel. siRNA). (**C**) Western blot analysis of Panc-1 total-cell lysates. One representative western blot of three independent experiments is shown HSC70 was used as loading control. (**D**) Quantification of western blots shown in (**C**) and additional replicates (n = 3). Mean ± SEM, one-way ANOVA (Dunnett's test), *p*-value relative to control group (Irrel. siRNA). (**E**) Western blot analysis of Panc-1 total-cell lysates. One representative western blot of three independent experiments is shown HSC70 was used as loading control. (**F**) Immunofluorescent confocal microscopy of Clathrin heavy chain upon myoferlin depletion in Panc-1 cells. Representative pictures are shown. Nuclei = blue, Clathrin heavy chain = green, scale bar = 20 µm.

relationship between myoferlin and focal adhesion in PDAC cells, we investigated whether myoferlin depletion impacts focal adhesion structure.

We demonstrated that myoferlin depletion in PDAC cells led to a reduction of focal adhesions number and to an accumulation of paxillin in the cytosol. Paxillin is a key adaptor protein that localizes to focal adhesions, where it interacts with multiple components (e.g., integrins, FAK, vinculin, talin) and plays a central role in focal adhesion assembly, signaling, and turnover. Since myoferlin-silencing reduced the number of focal adhesions, the availability of anchoring sites at the plasma membrane for paxillin binding is diminished, which may explain its cytosolic accumulation.

This report shows that myoferlin knockdown led, directly or indirectly, to a significant reduction in the amount of clathrin heavy chain. This reduction severely impaired or completely blocked clathrin-mediated endocytosis (CME), as suggested by the plasma membrane accumulation of integrins. CME is vital for internalizing various cell surface proteins including integrins and receptors. Indeed, it was previously demonstrated that myoferlin was involved in cell surface receptor recycling[22,35]. Integrins, which are the primary components of focal adhesions and mediate cell-extracellular matrix interactions, are constantly recycled between the plasma membrane and intracellular compartments. CME plays a crucial role in internalizing integrins from the cell surface. If integrin internalization via CME is impaired, integrins initially accumulate on the cell surface[36]. In the absence of a proper integrin trafficking, focal adhesion complexes cannot be effectively assembled at the plasma membrane, participating to the accumulation of focal adhesion components in the cytosol. However, this hypothesis is purely speculative and requires further investigation.

Cell migration is a highly coordinated process that relies on the precise assembly, maturation, and disassembly of focal adhesions. The reduction in functional focal adhesions means the cell has fewer points of stable attachment to the extracellular matrix. This directly impacts the cell ability to generate traction forces required for movement.

Since the discovery of myoferlin as an overexpressed protein in PDAC[3], several reports showed, in agreement with our results, its requirement for in vitro cell migration[9,10,12,22,34,37]. The clinical relevance of myoferlin in metastatic dissemination should be enhanced by validating our results in an in vivo model. Although this validation is not an integral part of our work, several reports demonstrate that this is indeed the case. In vivo, genetic interference with myoferlin expression resulted in a decrease in metastatic dissemination from breast[38] and pancreatic cancer cells[39]. Unfortunately, most of these studies did not propose a consistent mechanism for the migration or dissemination reduction.

Recently, the screening of a small compound library found, using canonical matrigel-coated transwell invasion assay as a readout, a series of compounds exhibiting anti-invasion activity. The molecular target of the lead compound (WJ460) was identified as myoferlin[8]. In an experimental metastasis murine model of breast cancer, this compound decreased significantly the development of lung metastasis and increased mice survival. Several related compounds were then designed and assayed with success in metastasis mice model, including from pancreatic cancer[9,10]. Considering the most water-soluble one (HJ445A), ADME (absorption, distribution, metabolism, excretion) properties were evaluated in vitro and in vivo[40]. It was noticeable that HJ445A slightly inhibited few CYP450 enzymes with micromolar IC50 and demonstrated little hERG-related cardiovascular toxicity. Due to the low to medium expression of myoferlin in normal adult tissue compared to malignant tissues, no toxicity was observed after 3 weeks of daily administration of HJ445A (30 mg/kg). Body weight was unchanged and histological examination of lung, liver, heart, kidney, spleen revealed no adverse effects[40].

Based on our findings, the critical steps of metastatic dissemination that most likely involve myoferlin are those that involve the dynamic assembly and disassembly of focal adhesions and the reorganization of actin microfilaments, particularly those that require cell movement and interaction with the extracellular matrix. These core steps of the metastatic cascade include the local invasion, the initial phase where tumor cells break away from the primary tumor and penetrate the surrounding tissue; the intravasation, the process by which a tumor cell enters the bloodstream or lymphatic vessels; and the extravasation, the process by which a tumor cell exits the bloodstream or lymphatic vessels.

In summary, we report a novel role of myoferlin during focal adhesion recycling in PDAC. The core of the proposed mechanism is that myoferlin knockdown primarily impairs clathrin-mediated endocytosis by reducing clathrin heavy chain. This defect then cascades, leading to dysfunctional integrin trafficking and focal adhesion dynamics, resulting in fewer focal adhesions, cytosolic accumulation of paxillin, and ultimately, a severe reduction in cell migration.

Data availability

The bulk RNAseq dataset analyzed during the current study is available in the Gene Expression Omnibus (GEO) repository, GSE306771 (https://www.ncbi.nlm.nih.gov/geo/query/acc.cgi?acc=GSE306771).

Received: 25 August 2025; Accepted: 31 October 2025
Published online: 28 November 2025

References

1. Filho, A. M. et al. The GLOBOCAN 2022 cancer estimates: Data sources, methods, and a snapshot of the cancer burden worldwide. *Int. J. Cancer* **156**, 1336–1346 (2025).
2. Bussetty, A. et al. Incidence of pancreas and colorectal adenocarcinoma in the US. *JAMA Netw. Open* **8**, e254682 (2025).
3. Turtoi, A. et al. Identification of novel accessible proteins bearing diagnostic and therapeutic potential in human pancreatic ductal adenocarcinoma. *J. Proteome Res.* **10**, 4302–4313 (2011).
4. Fahmy, K. et al. Myoferlin plays a key role in VEGFA secretion and impacts tumor-associated angiogenesis in human pancreas cancer. *Int. J. Cancer* **138**, 652–663 (2016).
5. Rademaker, G. et al. Myoferlin controls mitochondrial structure and activity in pancreatic ductal adenocarcinoma, and affects tumor aggressiveness. *Oncogene* **66**, 1–15 (2018).
6. Wang, W. S. et al. ITRAQ-based quantitative proteomics reveals myoferlin as a novel prognostic predictor in pancreatic adenocarcinoma. *J. Proteomics* **91**, 453–465 (2013).
7. Bernatchez, P. N., Sharma, A., Kodaman, P. & Sessa, W. C. Myoferlin is critical for endocytosis in endothelial cells. *Am. J. Physiol. Cell Physiol.* **297**, C484-92 (2009).
8. Zhang, T. et al. A small molecule targeting myoferlin exerts promising anti-tumor effects on breast cancer. *Nat. Commun.* **9**, 3726 (2018).
9. Li, Y. et al. Modification and biological evaluation of a series of 1,5-diaryl-1,2,4-triazole compounds as novel agents against pancreatic cancer metastasis through targeting myoferlin. *J. Med. Chem.* **62**, 4949–4966 (2019).
10. He, Y. et al. A potent and selective small molecule inhibitor of myoferlin attenuates colorectal cancer progression. *Clin. Transl. Medicine* **11**, e289 (2021).
11. Gu, H. et al. Discovery of 1,5-diaryl-1,2,4-triazole derivatives as myoferlin inhibitors and their antitumor effects in pancreatic cancer. *Futur. Med. Chem.* **14**, 1425–1440 (2022).
12. Rademaker, G. et al. Myoferlin contributes to the metastatic phenotype of pancreatic cancer cells by enhancing their migratory capacity through the control of oxidative phosphorylation. *Cancers* **11**, 853 (2019).
13. Rademaker, G. et al. Myoferlin targeting triggers mitophagy and primes ferroptosis in pancreatic cancer cells. *Redox Biol.* **53**, 102324 (2022).
14. Li, J. et al. Small molecule MMRi62 induces ferroptosis and inhibits metastasis in pancreatic cancer via degradation of ferritin heavy chain and mutant p53. *Mol. Cancer Ther.* **21**, 535–545 (2022).
15. Raphael, B. J. et al. Integrated genomic characterization of pancreatic ductal adenocarcinoma. *Cancer Cell* **32**, 185-203.e13 (2017).
16. Anania, S. et al. Identification of myoferlin as a mitochondria-associated membranes component required for calcium signaling in PDAC cell lines. *Cell Commun. Signal.* **22**, 133 (2024).
17. Wu, M. et al. Development and validation of a metastasis-related gene signature for predicting the overall survival in patients with pancreatic ductal adenocarcinoma. *J. Cancer* **11**, 6299–6318 (2020).
18. Barnhouse, V. R. et al. Myoferlin regulates epithelial cancer cell plasticity and migration through autocrine TGF-β1 signaling. *Oncotarget* **9**, 19209–19222 (2018).
19. Zaidel-Bar, R., Milo, R., Kam, Z. & Geiger, B. A paxillin tyrosine phosphorylation switch regulates the assembly and form of cell-matrix adhesions. *J. Cell Sci.* **120**, 137–148 (2007).
20. Woodrow, M. A., Woods, D., Cherwinski, H. M., Stokoe, D. & McMahon, M. Ras-induced serine phosphorylation of the focal adhesion protein paxillin is mediated by the Raf→MEK→ERK pathway. *Exp. Cell Res.* **287**, 325–338 (2003).
21. Cortesio, C. L., Boateng, L. R., Piazza, T. M., Bennin, D. A. & Huttenlocher, A. Calpain-mediated proteolysis of paxillin negatively regulates focal adhesion dynamics and cell migration. *J. Biol. Chem.* **286**, 9998–10006 (2011).
22. Turtoi, A. et al. Myoferlin is a key regulator of EGFR activity in breast cancer. *Cancer Res.* **73**, 5438–5448 (2013).
23. Nürnberg, A., Kitzing, T. & Grosse, R. Nucleating actin for invasion. *Nat. Rev. Cancer* **11**, 177–187 (2011).
24. Yadav, T., Gau, D. & Roy, P. Mitochondria–actin cytoskeleton crosstalk in cell migration. *J. Cell Physiol.* **237**, 2387–2403 (2022).
25. Fung, T. S., Chakrabarti, R. & Higgs, H. N. The multiple links between actin and mitochondria. *Nat. Rev. Mol. Cell Biol.* **24**, 651–667 (2023).
26. Altieri, D. C. Mitochondrial dynamics and metastasis. *Cell. Mol. Life Sci.* **76**, 827–835 (2019).
27. Ghosh, J. C. et al. Ghost mitochondria drive metastasis through adaptive GCN2/Akt therapeutic vulnerability. *Proc. Natl. Acad. Sci. U.S.A.* **119**, e2115624119 (2022).
28. Caino, M. C. et al. Syntaphilin controls a mitochondrial rheostat for proliferation-motility decisions in cancer. *J. Clin. Invest.* **127**, 3755–3769 (2017).
29. Agarwal, E. et al. Myc regulation of a mitochondrial trafficking network mediates tumor cell invasion and metastasis. *Mol. Cell. Biol.* **39**, e00109-19 (2019).
30. Li, G.-B. et al. Mitochondrial fission and mitophagy depend on cofilin-mediated actin depolymerization activity at the mitochondrial fission site. *Oncogene* **43**, 95 (2018).
31. Kruppa, A. J. et al. Myosin VI-dependent actin cages encapsulate parkin-positive damaged mitochondria. *Dev. Cell* **44**, 484-499.e6 (2018).
32. Blackstone, B. N. et al. Myoferlin depletion elevates focal adhesion kinase and paxillin phosphorylation and enhances cell-matrix adhesion in breast cancer cells. *Am. J. Physiol. Cell Physiol.* **308**, C642-9 (2015).
33. Volakis, L. I. et al. Loss of myoferlin redirects breast cancer cell motility towards collective migration. *PLoS ONE* **9**, e86110 (2014).
34. Zhang, W., Zhou, P., Meng, A., Zhang, R. & Zhou, Y. Down-regulating Myoferlin inhibits the vasculogenic mimicry of melanoma via decreasing MMP-2 and inducing mesenchymal-to-epithelial transition. *J. Cell. Mol. Med.* **155**, 739 (2017).
35. Demonbreun, A. R. et al. Myoferlin is required for insulin-like growth factor response and muscle growth. *Faseb J.* **24**, 1284–1295 (2010).
36. Ezratty, E. J., Bertaux, C., Marcantonio, E. E. & Gundersen, G. G. Clathrin mediates integrin endocytosis for focal adhesion disassembly in migrating cells. *J. Cell Biol.* **187**, 733–747 (2009).
37. Chen, X. et al. hnRNPLL regulates MYOF alternative splicing and correlates with early metastasis in pancreatic ductal adenocarcinoma. *Cancer Lett.* **611**, 217436 (2025).
38. Blomme, A. et al. Myoferlin regulates cellular lipid metabolism and promotes metastases in triple-negative breast cancer. *Oncogene* **36**, 2116–2130 (2017).
39. Li, Z. et al. Targeting MYOF suppresses pancreatic ductal adenocarcinoma progression by inhibiting ILF3-LCN2 signaling through disrupting OTUB1-mediated deubiquitination of ILF3. *Redox Biol.* **84**, 103665 (2025).

40. Gu, H. et al. Discovery of a highly potent and selective MYOF inhibitor with improved water solubility for the treatment of gastric cancer. *J. Med. Chem.* **66**, 16917–16938 (2023).

Acknowledgements
The results published here are in part based upon data generated by the TCGA Research Network: https://www.cancer.gov/tcga. The authors express their acknowledgement to the excellent support provided by the GIGA technical facilities (University of Liège). Notably Dr. Sandra Ormenese with M. Alexandre Hego and M. Gaëtan Lefevre from the GIGA-Imaging platform, and Dr. Arnaud Lavergne from GIGA-Bioinformatics platform.

Author contributions
C.G., E.L., M.D., F.A., N.M., M.T. acquired data. C.G., E.L., R.P., Y.B., D.L., A.B., M.T., G.R, O.P. participated in data analysis and interpretation. G.R., O.P. contributed to the conception and design of the work. O.P. wrote the main manuscript and prepared the figures. G.R., R.P., E.L. edited the manuscript. All authors revised and approved the final version of the manuscript.

Funding
This work was supported by the "Fondation Léon Frédericq", the Julia Russe prize, the University of Liège "crédits sectoriels (CSRV-SS)". RP is a Research Fellow (FNRS, grant N° 40010385), GR is a Postdoctoral Researcher (FNRS, grant N° 40024125), AB is a Research Director (FNRS).

Declarations

Competing interests
The authors declare no competing interests.

Ethical approval
Not applicable.

Additional information
Supplementary Information The online version contains supplementary material available at https://doi.org/10.1038/s41598-025-27134-2.

Correspondence and requests for materials should be addressed to O.P.

Reprints and permissions information is available at www.nature.com/reprints.

Publisher's note Springer Nature remains neutral with regard to jurisdictional claims in published maps and institutional affiliations.